

Generating large-scale Greenberger-Horne-Zeilinger-like states in lattice spin systems

Xuanchen Zhang,^{1,*} Yaofeng Chen,^{1,*} and Yong-Chun Liu^{1,2,†}

¹*State Key Laboratory of Low-Dimensional Quantum Physics,*

Department of Physics, Tsinghua University, Beijing 100084, China

²*Frontier Science Center for Quantum Information, Beijing 100084, China*

(Dated: February 26, 2026)

Greenberger-Horne-Zeilinger (GHZ) state is a typical maximally entangled state which is pursued in both fundamental research and emerging quantum technologies. Preparing large-scale GHZ states in lattice spin systems is particularly appealing for quantum advantages, but conventional schemes face great challenges in scalability. Here we propose a universal and scalable scheme to generate large-scale GHZ-like states, which share similar entanglement and metrological properties with standard GHZ states, in lattice spin systems through global Floquet engineering. Our scheme requires only global operations and shows great advantage for large particle number. It is applicable to systems with arbitrary interaction ranges, offering a practical pathway for large-scale implementation of many-body entangled states in various systems.

I. INTRODUCTION

Lattice spin systems have emerged as promising platforms for quantum computation [1–3], quantum simulation [4–6], and quantum metrology [7–9], owing to their advantages in addressability and control. Central to these applications is the ability to create large-scale non-classical states with many-body entanglement, which is a key resource in the pursuit of quantum advantages [10, 11]. A typical example is scalable spin-squeezed states [12–22], which enable quantum-enhanced metrology [23–28] and have recently been widely investigated in lattice spin platforms [29–36]. A more ambitious target is the Greenberger-Horne-Zeilinger (GHZ) state [37], which is a representative example of maximally entangled state. They are not only crucial in quantum technologies such as quantum precision measurement [38, 39], but also play vital roles in fundamental researches covering macroscopic quantum effects [40] and quantum non-locality [37, 41]. Experimentally, GHZ states have been realized across various systems, including superconducting circuits [42–44], trapped ions [45, 46], Rydberg atom arrays [47], and photonic systems [48, 49].

However, previous schemes for generating GHZ states encounter significant challenges in scalability. Typically, GHZ states are prepared either through sequences of two-qubit gates [50–52] or via optimal control involving evolution in full Hilbert space [47, 53, 54]. These approaches have limitations for large particle number due to the accumulation of errors in gate operation and increase of complexity in optimal control. These constraints significantly impede the broader exploitation of GHZ states in fundamental quantum researches and emerging quantum technologies.

In this work, we present a universal and scalable scheme to generate large-scale GHZ-like states in lat-

tice spin systems via global Floquet engineering. The generated GHZ-like states are similar to standard GHZ states in entanglement and metrological properties. Considering the power-law Ising model, we find that the effective interaction induced by a periodic sequence of global single-qubit rotations includes a collective-spin three-body term, which can create GHZ-like states for large particle number. The spin-wave excitations can be suppressed by reducing the separation between the rotation pulses, making our scheme applicable to extensive interaction ranges. We further take into account typical incoherent noises and demonstrate the robustness of our scheme against decoherence.

II. SYSTEM MODEL AND OUR SCHEME

We consider the power-law Ising model with the interaction described by

$$H = \sum_{j \neq k} K_{jk} s_j^z s_k^z, \quad (1)$$

where $s_j^z = \sigma_j^z/2$ is the z component of the j -th spin, and the coupling strength between spins j and k located at positions \mathbf{r}_j and \mathbf{r}_k is given by

$$K_{jk} = K/|\mathbf{r}_j - \mathbf{r}_k|^\alpha, \quad (2)$$

with K being the interaction strength of the nearest-neighbor pair and α being the decaying factor. In this paper, we focus on the cases of 1-dimensional (1D) and 2-dimensional (2D) square lattices. Such a model can be realized in a variety of lattice spin systems including trapped ions ($0 < \alpha < 3$) [55, 56], Rydberg atom arrays ($\alpha = 3, 6$) [57, 58], polar molecules ($\alpha = 3$) [59], superconducting circuits ($\alpha \rightarrow \infty$, the limit of nearest-neighbor interactions) [60], and others. Note that the Hamiltonian (1) reduces to the well-known one-axis twisting (OAT) model [12]

$$H_{\text{OAT}} = K(S_z^2 - N/2), \quad (3)$$

* These authors contributed equally.

† ycliu@tsinghua.edu.cn

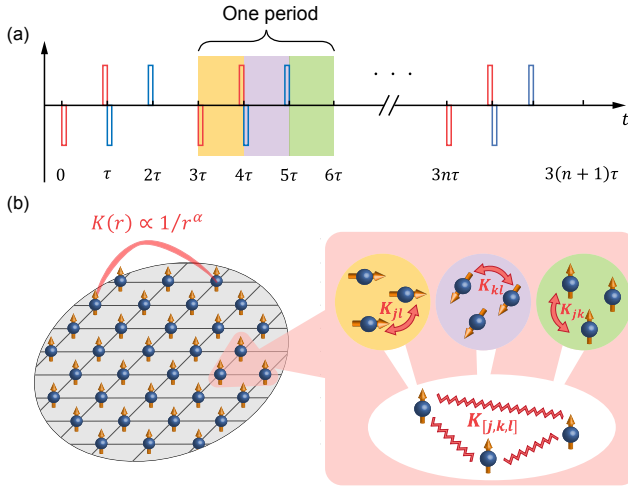


FIG. 1. Schematic diagram of the scheme to generate GHZ-like states in lattice spin systems governed by the power-law Ising model. (a) An illustration of the pulse sequences. The red and blue pulses denote $\pm\pi/2$ pulses along x and y axis, respectively. The spins effectively interact through $s_j^y s_k^y$ (yellow shaded), $s_j^x s_k^x$ (purple shaded) and $s_j^z s_k^z$ (green shaded) in the three successive parts of one period, each taking the time of τ . (b) An illustration of the model. The spins located in a square lattice interact through power-law Ising interaction, with interaction strength decaying with distance r as $1/r^\alpha$. The noncommutativity of the three segments in one period gives rise to the effective three-body interaction.

when interactions are uniform ($\alpha = 0$), which are often referred to as all-to-all or infinite-range interactions, where $S_z = \sum_{i=1}^N s_i^z$ denotes the z component of the collective spin operator \mathbf{S} with total spin $S = N/2$, and N is the total particle number.

To generate GHZ-like states, we introduce the global Floquet-driving scheme involving iterative $\pi/2$ pulses along x - and y -axes [61], as shown in Fig. 1(a). The evolution operator over one period is given by

$$U(3\tau) = e^{-iH\tau} e^{-i\frac{\pi}{2}S_y} e^{-iH\tau} e^{i\frac{\pi}{2}S_y} e^{-i\frac{\pi}{2}S_x} e^{-iH\tau} e^{i\frac{\pi}{2}S_x} \\ = e^{-iH_{zz}\tau} e^{-iH_{xx}\tau} e^{-iH_{yy}\tau}, \quad (4)$$

where $H_{\mu\mu} = \sum_{j \neq k} K_{jk} s_j^\mu s_k^\mu$ ($\mu = x, y, z$), and τ denotes the separation between two $\pm\pi/2$ pulses. This pulse sequence effectively engineers spin-spin interactions of the forms $s_j^y s_k^y$, $s_j^x s_k^x$ and $s_j^z s_k^z$ in the three segments of each cycle, respectively. For sufficiently small τ , the evolution operator can be approximated as

$$U(3\tau) = \exp \left\{ -i3\tau H_{\text{eff}} + \mathcal{O}(\tau^2) \right\}, \quad (5)$$

where the effective Hamiltonian is obtained using the Baker-Campbell-Hausdorff expansion and takes the form

(see Appendix A for detailed derivations)

$$H_{\text{eff}} = \frac{1}{3} \sum_{j \neq k} K_{jk} \mathbf{s}_j \cdot \mathbf{s}_k \\ + \frac{1}{3} \tau \sum_{[j,k,l]} K_{[j,k,l]} (s_j^x s_k^y s_l^z + s_l^z s_k^y s_j^x), \quad (6)$$

where $[j, k, l]$ stands for a combination of mutually distinct indices j, k, l , and the effective three-body interaction strength is given by

$$K_{[j,k,l]} = K_{jl}K_{kl} + K_{jk}K_{lk} - K_{kj}K_{lj}. \quad (7)$$

The requirement for safely ignoring higher order terms $\mathcal{O}(\tau^2)$ imposes the condition $\tau \ll \tau_{\text{crit}} \sim L^{-\max(0, d-\alpha)}$ for d -dimensional square lattice with lattice length L .

The effective Hamiltonian (6) consists of two terms with clear physical interpretations. The zeroth-order term corresponds to the Heisenberg coupling $\mathbf{s}_j \cdot \mathbf{s}_k = s_j^x s_k^x + s_j^y s_k^y + s_j^z s_k^z$, which induces a many-body gap between the permutationally symmetric manifold (the Dicke manifold) and the others, thus suppresses the leakage of population outside the Dicke manifold. The first-order term is the effective three-body interaction originated from the noncommutativity of three segments within one Floquet period, as shown in Fig. 1(b). Crucially, the protection provided by the Heisenberg coupling effectively retains the collective part of this term, which is the key mechanism enabling the generation of GHZ-like states in our scheme.

III. ZERO-MOMENTUM/FINITE-MOMENTUM DECOMPOSITION

In this section, we study the effective Hamiltonian (6) by applying the zero-momentum/finite-momentum decomposition [62]. This treatment serves to demonstrate explicitly that our scheme can generate GHZ-like states and to identify the corresponding parameter regime.

We begin by introducing the Holstein-Primakoff (HP) transformation

$$s_j^x = \frac{1}{2} \left(\sqrt{1 - b_j^\dagger b_j} b_j + b_j^\dagger \sqrt{1 - b_j^\dagger b_j} \right), \\ s_j^y = \frac{1}{2i} \left(\sqrt{1 - b_j^\dagger b_j} b_j - b_j^\dagger \sqrt{1 - b_j^\dagger b_j} \right), \\ s_j^z = \frac{1}{2} - b_j^\dagger b_j. \quad (8)$$

Exploiting the translational symmetry of the system, it is convenient to define the HP bosons in momentum space

$$b_{\mathbf{q}} = \sum_j e^{-i\mathbf{q} \cdot \mathbf{r}_j} / \sqrt{N}, \quad (9)$$

with momentum vectors $\mathbf{q} = 2\pi(q_1, q_2, \dots, q_d)/L$, where $q_m = 0, 1, \dots, L-1$.

For a generic operator O , we decompose it into zero- and finite-momentum components

$$O = [O]_{\text{ZM}} + [O]_{\text{FM}}. \quad (10)$$

The zero-momentum component contains only $q = 0$ HP bosons, $[O]_{\text{ZM}} = [O]_{\text{ZM}}(b_0, b_0^\dagger)$, which is exactly the permutationally symmetric part and can be calculated by projecting O onto the Dicke manifold $\{|S = N/2, M\rangle \equiv |M\rangle\}$ [62]:

$$[O]_{\text{ZM}} = \sum_{M, M'} \langle M|O|M'\rangle |M\rangle \langle M'|. \quad (11)$$

By contrast, the finite-momentum component $[O]_{\text{FM}}$ describes the non-collective fluctuations. Provided these fluctuations remain small during the whole evolution, they can be treated perturbatively by retaining up to quadratic terms of the bosonic operators $b_{\mathbf{q}}^2$, $b_{\mathbf{q}}^{\dagger 2}$ and $b_{\mathbf{q}}^\dagger b_{\mathbf{q}}$.

Applying this decomposition to the effective Hamiltonian (6), we approximately split it into two independent parts (see Appendix B):

$$H_{\text{eff}} \simeq H_{\text{ZM}} + H_{\text{SW}}. \quad (12)$$

The zero-momentum component takes exactly the form of the collective-spin cubic XYZ model as defined in [61]:

$$H_{\text{ZM}} = \frac{1}{3} \lambda K^2 \tau (J_x J_y J_z + J_z J_y J_x), \quad (13)$$

where $J_\mu = \sum_{M, M'} |M\rangle \langle M| S_\mu |M'\rangle \langle M'|$ is the zero-momentum component of the collective-spin operator S_μ , which has a fixed spin length $J = N/2$. This Hamiltonian governs the purely collective dynamics within the Dicke manifold and is responsible for the generation of GHZ-like states. The finite-momentum component, up to quadratic terms of the HP bosons, corresponds to the spin-wave Hamiltonian

$$H_{\text{SW}} = -\frac{N}{12} K_0 + \frac{1}{3} \sum_{\mathbf{q} \neq 0} (K_0 - K_{\mathbf{q}}) b_{\mathbf{q}}^\dagger b_{\mathbf{q}} - i \frac{\tau}{12} \sum_{\mathbf{q} \neq 0} (K_{\mathbf{q}}^2 - T_0^2) (b_{\mathbf{q}} b_{-\mathbf{q}} - b_{\mathbf{q}}^\dagger b_{-\mathbf{q}}^\dagger), \quad (14)$$

where the coefficients are defined as

$$\lambda = \frac{1}{N(N-1)(N-2)} \sum_{[j,k,l]} \frac{1}{r_{jl}^\alpha} \frac{1}{r_{kl}^\alpha}, \quad K_{\mathbf{q}} = K \sum_{\mathbf{r} \neq 0} \frac{1}{r^\alpha} e^{-i\mathbf{q}\cdot\mathbf{r}}, \quad T_0^2 = K^2 \sum_{\mathbf{r} \neq 0} \frac{1}{r^{2\alpha}}. \quad (15)$$

The undesired non-collective effects are described by the linear spin-wave excitations, which can be exactly solved via the Bogoliubov diagonalization of H_{SW} (14), leading to (see Appendix B)

$$\langle b_{\mathbf{q}}^\dagger b_{\mathbf{q}} \rangle(t) = \frac{\tau^2}{2} \frac{B_{\mathbf{q}}^2}{A_{\mathbf{q}}^2 - \tau^2 B_{\mathbf{q}}^2} [1 - \cos(\epsilon_{\mathbf{q}} t)], \quad (16)$$

with $A_{\mathbf{q}} = (K_0 - K_{\mathbf{q}})/3$, $B_{\mathbf{q}} = (K_{\mathbf{q}}^2 - T_0^2)/6$ and $\epsilon_{\mathbf{q}} = \sqrt{A_{\mathbf{q}}^2 - \tau^2 B_{\mathbf{q}}^2}$.

The above decomposition neglects both the nonlinear behavior of the finite-momentum component and its coupling to the zero-momentum component. This approximation is reasonable as long as the finite-momentum excitations remain weak. From Eq. (16), we find that a sufficiently small pulse separation $\tau \ll \min_{\mathbf{q}} [A_{\mathbf{q}}/B_{\mathbf{q}}]$ is able to suppress the finite-momentum spin-wave excitations. Once this condition is fulfilled, the evolution will be dominated by the zero-momentum component H_{ZM} (13), generating a GHZ-like state from an initial coherent spin state [61].

IV. NUMERICAL INVESTIGATION

In this section, we investigate the performance of our scheme by numerically studying the time evolution governed by Eq. (4).

A. Characterizing the GHZ-like state

Choosing the initial state as the coherent spin state polarized along z -axis $|\psi(0)\rangle = |\uparrow\rangle^{\otimes N}$, our scheme creates a GHZ-like state with probability distribution strongly concentrated near the extremal eigenvalues $S_x = \pm N/2$. As representative examples, we consider a 1-dimensional (1D) system of 20×1 spins with $\alpha = 1$, and a 2D system of 4×4 spins with $\alpha = 3$. The resulting probability distributions $P(m) \equiv P(S_x = m)$ of the obtained states are shown in Fig. 2 (a1) and (b1). In both cases, the distributions are clearly bimodal, with most of the weight concentrated near $S_x = \pm N/2$, indicating the formation of collective superpositions.

The coherence of GHZ-like states can be further demonstrated by examining the parity operator

$$\Pi(\theta) = e^{-iS_x \theta} \left(\prod_{i=1}^N \sigma_i^z \right) e^{iS_x \theta}. \quad (17)$$

For an ideal GHZ state, the expectation value of the parity exhibits high-frequency oscillations,

$$\langle \Pi(\theta) \rangle_{\text{GHZ}} = \cos N\theta. \quad (18)$$

In Fig. 2 (a2) and (b2) We plot parity oscillations of the numerically obtained states. The observed oscillatory behavior closely follows the ideal GHZ pattern, confirming the GHZ-like nature of the generated states in our scheme.

For larger systems, full quantum simulations become impractical. Fortunately, the emergence of the GHZ-like state can also be revealed by the time evolution of quantum Fisher information (QFI) in regard to the generator

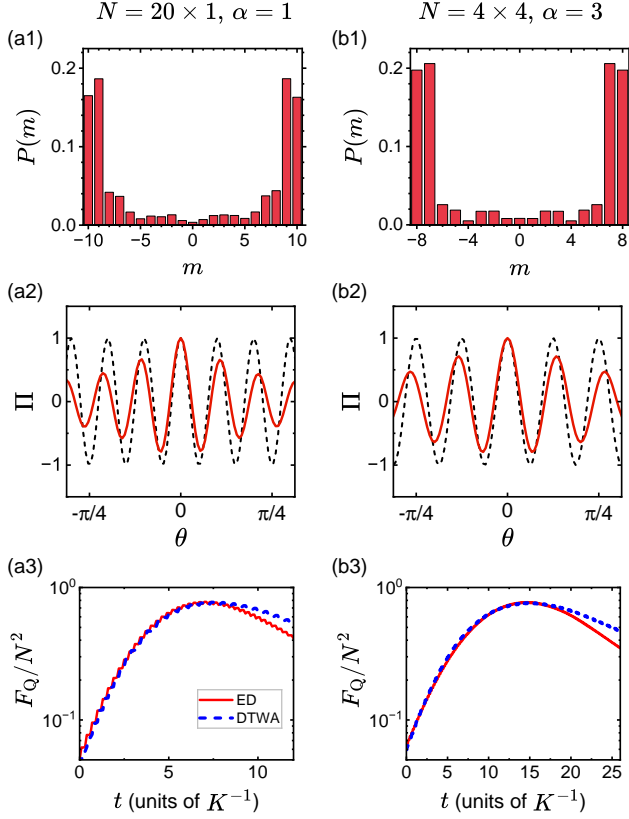


FIG. 2. Characterization of the GHZ-like state generated in our scheme, calculated for (a) 20×1 spins, $\alpha = 1$, $K\tau = 0.1$ and (b) 4×4 spins, $\alpha = 3$, $K\tau = 0.06$. (a1), (b1) The probability distributions $P(m)$ of the obtained states, where m denotes the eigenvalue of S_x . (a2), (b2) Parity oscillations of the obtained states. Black dashed curves show the results of perfect GHZ states $\langle \Pi(\theta) \rangle_{\text{GHZ}} = \cos N\theta$. (a3), (b3) Time evolution of the quantum Fisher information F_Q , obtained using exact diagonalization (ED, red solid) and discrete truncated Wigner approximation (DTWA, blue dashed).

S_x , which is proportional to the spin fluctuation along x -axis for pure states:

$$F_Q^{S_x}(|\psi\rangle) = 4(\Delta S_x)_{|\psi\rangle}^2. \quad (19)$$

It quantifies the minimum uncertainty to measure the unknown parameter ϕ of a perturbation $e^{iS_x\phi}$, namely the quantum Cramér-Rao bound

$$\frac{1}{(\Delta\phi)^2} \leq F_Q^{S_x}. \quad (20)$$

The QFI of GHZ-like states should approach the Heisenberg limit $F_Q = N^2$. To numerically study it in large systems, we resort to the discrete truncated Wigner approximation (DTWA) [63]. This semi-classical approach reliably reproduces the time evolution of QFI over the time scales relevant to our study, as demonstrated for small systems in Fig. 2 (a3) and (b3). In the

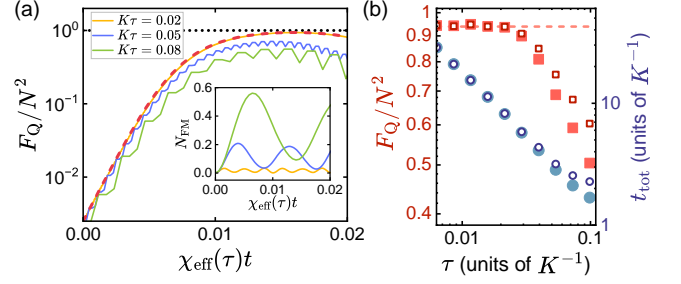


FIG. 3. The influence of the pulse separation τ on the evolution for 2D lattice of 20×20 spins with decaying factor $\alpha = 2$. (a) The time evolution of the QFI F_Q for different pulse separations, compared with the result of the zero-momentum Hamiltonian H_{ZM} (red dashed curve) and the Heisenberg limit $F_Q = N^2$ (black dotted line). The time evolution of finite-momentum spin-wave excitation N_{FM} is shown in the inset. Here the evolution time has been rescaled with a factor $\chi_{\text{eff}}(\tau) = \lambda N K^2 \tau / 6$. (b) The maximal QFI (red square) and the corresponding total evolution time t_{tot} (blue circle) versus the pulse separation τ . Open squares (circles) denote the optimal QFI over all generator directions F_Q^{opt} (and the corresponding evolution time), whereas solid squares (circles) correspond to the QFI in regard to the generator S_x , $F_Q^{S_x}$ (and the corresponding evolution time). The red dashed line indicates the maximal $F_Q^{S_x}$ of the zero-momentum Hamiltonian. The QFI is obtained using the DTWA (averaged over 1000 trajectories).

following sections, we apply DTWA to systematically investigate the performance of our scheme across a wide range of system sizes.

B. The influence of the pulse separation

As discussed in Sec. III, the pulse separation τ plays a vital role to suppress the finite-momentum spin-wave excitations, thereby restoring the dynamics to the collective-spin regime. Here we provide explicit numerical evidence for this effect. In Fig. 3(a), considering a 2D lattice of 20×20 spins with interaction decaying factor $\alpha = 2$, we plot the time evolution of QFI and the total finite-momentum spin-wave excitation

$$N_{\text{FM}} = \sum_{\mathbf{q} \neq 0} \langle b_{\mathbf{q}}^\dagger b_{\mathbf{q}} \rangle, \quad (21)$$

for different pulse separations τ . It clearly shows that, as τ decreases, N_{FM} becomes smaller, and the evolution of the QFI therefore gets closer to that of the effective collective-spin cubic XYZ model determined by H_{ZM} (13), with the peak value approaching the Heisenberg limit $F_Q = N^2$.

The dependence of the maximal QFI and the corresponding total evolution time t_{tot} on the pulse separation τ is provided in Fig. 3(b). It reveals that when the pulse separation τ is small enough, the maximal QFI perfectly matches that of the collective-spin cubic XYZ model. On

the other hand, as the effective interaction strength is proportional to τ , the total evolution time t_{tot} becomes longer for a smaller τ . As a result, there is a trade-off between the high-fidelity and fast generation of GHZ-like state, and it is crucial to choose a suitable τ to ensure the GHZ-like state generation is fast and efficient.

In addition, we note that the optimal QFI over all generator directions, $F_Q^{\text{opt}} = \max_n (F_Q^{S_n})$, can be determined via the QFI-matrix approach [64]. In Fig. 3(b) we also show F_Q^{opt} and the corresponding optimal evolution time. In the small- τ regime, F_Q^{opt} match perfectly with $F_Q^{S_x}$, indicating that S_x is the optimal generator. For larger τ , F_Q^{opt} becomes slightly larger than $F_Q^{S_x}$, but their overall behavior remains consistent and leads to no qualitative difference. We therefore conclude that $F_Q^{S_x}$ provides an accurate and practical characterization of the optimal metrology performance of the states generated in our scheme. In the remainder of this work, we focus exclusively on $F_Q^{S_x}$.

C. Scaling behavior

To identify a suitable τ in our scheme, we consider a characteristic pulse separation τ_s at which the ratio F_Q/F_Q^{eff} reaches a given threshold, where F_Q^{eff} is the QFI achieved by the effective collective-spin cubic XYZ model (13). This ratio quantifies the metrological similarity between the generated states under the synthesized Hamiltonian (6) and those of H_{ZM} (13). Here we use $F_Q/F_Q^{\text{eff}} = 0.8$ to study how τ_s scales with the length of the lattice L for different decay factor α and dimension d . We note that other choices with different F_Q/F_Q^{eff} give similar results (see Appendix E).

From the numerical results we find that the relation between τ_s and L approximately follows a power-law form $\tau_s \sim L^{-\mu}$, corresponding to the fitted black dashed line in Fig. 4(a1) and (b1). In Fig. 4(a2) and (b2), we plot the numerically fitted μ as a function of α . We can observe an evident transition at $\alpha = d$, which is often seen as the critical point that separates short-range and long-range interactions. Remarkably, even for short-range interactions with very large α , our scheme still works and the power-law exponent μ approaches to 2.

We can gain intuition for the above scaling behavior from the requirement $\tau \ll \min_{\mathbf{q}}[A_{\mathbf{q}}/B_{\mathbf{q}}]$, which implies the scaling law of τ_s should follow that of $\min_{\mathbf{q}}[A_{\mathbf{q}}/B_{\mathbf{q}}]$. Approximating the summations by integrals, we obtain $\tau_s \sim L^{-\mu}$ with (see Appendix C)

$$\mu = \begin{cases} d - \alpha & \alpha < d, \\ \alpha - d & d < \alpha < d + 2, \\ 2 & \alpha \geq d + 2. \end{cases} \quad (22)$$

This matches well with the numerical results as shown in Fig. 4(a2) and (b2) for most parameter ranges. One

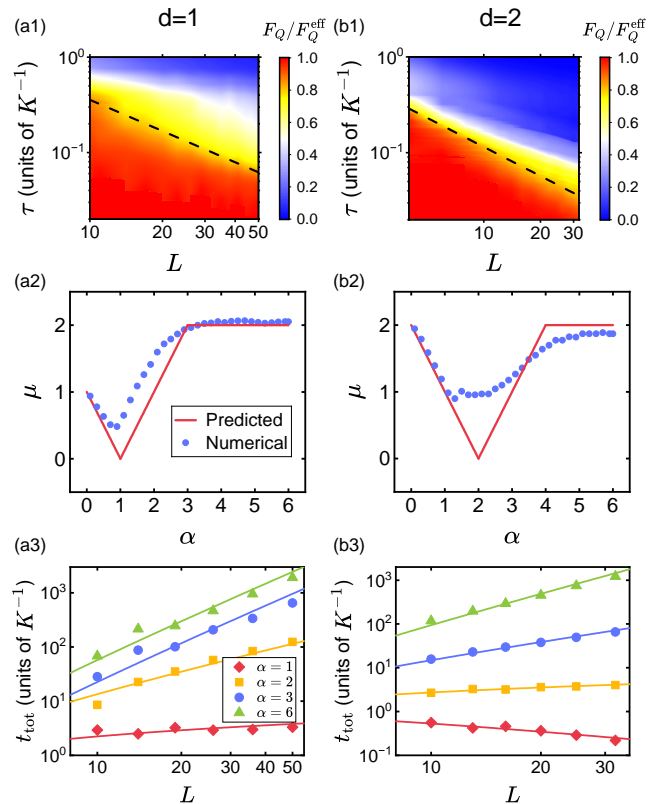


FIG. 4. The performance of the scheme versus different lattice length L , pulse separation τ and decaying factor α for (a) 1D and (b) 2D lattices. (a1, b1) The ratio between the maximal quantum Fisher information of the scheme and the effective one (H_{ZM}) F_Q/F_Q^{eff} as a function of L and τ , calculated at $\alpha = 1.5$. The black dashed line shows the fitting result of $F_Q/F_Q^{\text{eff}} = 0.8$. (a2, b2) The power-law exponent μ of the suitable pulse separation τ_s which approximately obeys $\tau_s \sim L^{-\mu}$, changing with α . Both the numerical fitting results (blue circle) and the value predicted by finite-momentum spin-wave excitations as Eq. (22) (red solid line) are presented. (a3, b3) The total evolution time as a function of L for different α , compared with the fitted scaling law $t_{\text{tot}} \sim L^{-\nu} \ln L$ with ν given by Eq. (23) (solid lines with corresponding colors). Numerical results are obtained using the DTWA (averaged over 1000 trajectories).

exception is the transition point near $\alpha = d$, where the dependence changes into a logarithmic one $\tau_s(\alpha = d) \sim (\ln L)^{-2}$.

After determining the pulse separation τ_s , we can obtain the required evolution time t_{tot} for generating GHZ-like states, with the results plotted in Fig. 4(a3) and (b3). For its scaling, we can deduce $t_{\text{tot}} \sim L^{-\nu} \ln L$ with (see Appendix D)

$$\nu = \begin{cases} d - \alpha & \alpha < d + 2, \\ -2 & \alpha \geq d + 2. \end{cases} \quad (23)$$

We can see the fitted scaling law with ν given by (23) indeed captures the behavior of t_{tot} . Notably, for some

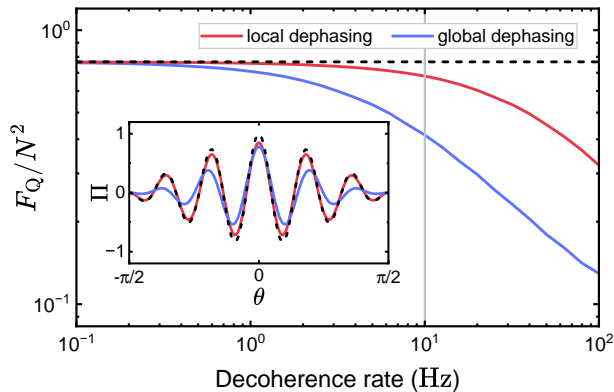


FIG. 5. The maximal QFI as a function of the decoherence rate for both local (γ) and global dephasing (Γ), evaluated under the proposed experimental parameters ($N = 12$ spins in 1D lattice, $K = 560$ Hz, and $\alpha = 1.0$). The pulse separation is fixed at $\tau = 0.18$ ms. The black dashed line represents the ideal case without decoherence. Inset: expectation value of the parity $\Pi = \prod_{j=1}^N \sigma_j^z$ after applying $e^{i\theta S_x}$, calculated at a decoherence rate of 10 Hz (gray line). Calculations are based on the exact diagonalization.

parameter ranges, t_{tot} becomes shorter as L increases, which is especially useful for generating large-scale GHZ-like states in terms of overcoming dissipations. From Eq. (23), we can find that this requires $\alpha < (d - 1/\ln L) \simeq d$. Therefore, if the interaction decaying factor is smaller than the system dimension, fast generation of large-scale GHZ-like states is promising.

V. ANALYSIS OF DECOHERENCE

The preparation of entangled states are often impeded by decoherence in real experiments. In this section, we analyse the potential impact of decoherence by modeling the system dynamics with a Lindblad master equation

$$\frac{d\hat{\rho}}{dt} = -i[H, \hat{\rho}] + \sum_j \left(L_j \hat{\rho} L_j^\dagger - \frac{1}{2} \{L_j^\dagger L_j, \hat{\rho}\} \right). \quad (24)$$

We focus on two representative types of incoherent noise commonly encountered in experiments: uniformed local dephasing described by the Lindblad operators $L_j = \sqrt{\gamma} s_j^z$, and global dephasing characterized by a collective Lindblad operator $L = \sqrt{\Gamma} S_z$. We adopt the experimental parameters of a trapped-ion system as reported in Ref. [35], and vary the decoherence rate of each type of noise respectively.

In open systems, the QFI of a mixed state $\hat{\rho}$ with re-

spect to the generator S_x is evaluated as

$$F_Q^{S_x}(\hat{\rho}) = 2 \sum_{q_\kappa + q_{\kappa'} > 0} \frac{(q_\kappa - q_{\kappa'})^2}{q_\kappa + q_{\kappa'}} |\langle \kappa' | S_x | \kappa \rangle|^2, \quad (25)$$

where $\hat{\rho} = \sum_\kappa q_\kappa |\kappa\rangle \langle \kappa|$ denotes the spectral decomposition of the density matrix. We perform full quantum simulation of the master equation (24) to calculate the QFI, presenting the impact of decoherence in Fig. 5.

As shown in Fig. 5, local dephasing has a relatively weaker impact as compared to global dephasing. This behavior is expected, since the off-diagonal matrix element $\langle \downarrow \dots \downarrow \hat{\rho} | \uparrow \dots \uparrow \rangle$ decays as $e^{-\gamma N t/2}$ for local dephasing, whereas global dephasing leads to a much faster decay $e^{-\Gamma N^2 t/2}$, with an additional factor N arising from the collective coupling to the environment. Furthermore, we find the parity oscillations remain well-resolved despite the presence of moderate decoherence, highlighting the robustness of our scheme against decoherence.

VI. CONCLUSION

In summary, we explore the scheme for the generation of large-scale GHZ-like states in lattice spin systems governed by the power-law Ising model. By utilizing a periodic sequence of global single-qubit rotational pulses, we can synthesize both three-body interactions and Heisenberg interactions. The three-body interactions lead to the creation of GHZ-like states, while the Heisenberg interactions protect the state evolution in the collective-spin subspace and thus facilitate the generation of GHZ-like states regardless of the interaction range. We numerically investigate the scaling behavior of both the suitable pulse separation and the total evolution time for generating the GHZ-like states, which is intuitively explained by analytically studying finite-momentum spin-wave excitations. The examination of the performance of our scheme under different types of decoherence support its robustness. This work presents a universal and scalable scheme to generate large-scale GHZ-like states in lattice spin systems, implementable on a variety of existing platforms with state-of-the-art experimental techniques.

ACKNOWLEDGMENTS

This work is supported by the National Key R&D Program of China (Grant No. 2023YFA1407600), the National Natural Science Foundation of China (NSFC) (Grants No. 92576204, No. 12275145, No. 92050110, No. 91736106, No. 11674390, and No. 91836302) and Beijing Key Laboratory of Quantum Artificial Intelligence.

DATA AVAILABILITY

The code that supports the findings of the article are openly available [65].

Appendix A: Derivation of the effective Hamiltonian

Assuming a sufficiently small pulse separation τ , we can expand the evolution operator (4) using the Baker-Campbell-Hausdorff (BCH) formula

$$e^{\epsilon A} e^{\epsilon B} = \exp \left\{ \epsilon(A+B) + \frac{1}{2} \epsilon^2 [A, B] + \mathcal{O}(\epsilon^3) \right\}, \quad (\text{A1})$$

which gives

$$\begin{aligned} U(3\tau) &= \exp \left\{ -i\tau(H_{zz} + H_{xx}) + \frac{1}{2} (-i\tau)^2 [H_{zz}, H_{xx}] + \mathcal{O}(\tau^3) \right\} \exp \{-i\tau H_{yy}\} \\ &= \exp \left\{ -i\tau(H_{zz} + H_{xx} + H_{yy}) + \frac{1}{2} (-i\tau)^2 ([H_{zz}, H_{xx}] + [H_{zz}, H_{yy}] + [H_{xx}, H_{yy}]) \right\}. \end{aligned} \quad (\text{A2})$$

The commutators appearing in the 2nd-order term can be calculated as follows:

$$\begin{aligned} [H_{xx}, H_{yy}] &= \sum_{j \neq k} \sum_{m \neq n} K_{jk} K_{mn} [s_j^x s_k^x, s_m^y s_n^y] \\ &= \sum_{j \neq k} \sum_{m \neq n} K_{jk} K_{mn} (s_j^x s_m^y [s_k^x, s_n^y] + s_j^x [s_k^x, s_m^y] s_n^y + [s_j^x, s_m^y] s_n^y s_k^x + s_m^y [s_j^x, s_n^y] s_k^x) \\ &= i \sum_{j \neq k} \sum_{m \neq n} K_{jk} K_{mn} (s_j^x s_m^y s_k^z \delta_{k,n} + s_j^x s_k^z s_n^y \delta_{k,m} + s_j^z s_n^y s_k^x \delta_{j,m} + s_m^y s_j^z s_k^x \delta_{j,n}) \\ &= 2i \sum_{[j,k,l]} K_{jl} K_{kl} (s_j^x s_k^y s_l^z + s_l^z s_k^y s_j^x), \end{aligned} \quad (\text{A3})$$

where the $[j, k, l]$ stands for a combination of mutually unequal j, k, l . During the derivation we have used $[s_j^\alpha, s_k^\beta] = i\delta_{jk} \sum_\gamma \epsilon_{\alpha\beta\gamma} s_j^\gamma$ and $\{s_j^\alpha, s_j^\beta\} = \delta_{\alpha\beta}/2$ for spin-1/2. Similarly we obtain

$$\begin{aligned} [H_{zz}, H_{xx}] &= 2i \sum_{[j,k,l]} K_{jk} K_{lk} (s_j^x s_k^y s_l^z + s_l^z s_k^y s_j^x), \\ [H_{zz}, H_{yy}] &= -2i \sum_{[j,k,l]} K_{kj} K_{lj} (s_j^x s_k^y s_l^z + s_l^z s_k^y s_j^x). \end{aligned} \quad (\text{A4})$$

The evolution operator then reads

$$U(3\tau) = \exp \left\{ -i\tau \left(\sum_{j \neq k} K_{jk} \mathbf{s}_j \cdot \mathbf{s}_k + \tau \sum_{[j,k,l]} K_{[j,k,l]} (s_j^x s_k^y s_l^z + s_l^z s_k^y s_j^x) \right) + \mathcal{O}(\tau^3) \right\}, \quad (\text{A5})$$

where $K_{[j,k,l]} = K_{jl} K_{kl} + K_{jk} K_{lk} - K_{kj} K_{lj}$. Since $U(3\tau) = \exp\{-i3\tau H_{\text{eff}} + \mathcal{O}(\tau^3)\}$, we obtain the effective Hamiltonian

$$\begin{aligned} H_{\text{eff}} &= \frac{1}{3} \sum_{j \neq k} K_{jk} \mathbf{s}_j \cdot \mathbf{s}_k \\ &\quad + \frac{1}{3} \tau \sum_{[j,k,l]} K_{[j,k,l]} (s_j^x s_k^y s_l^z + s_l^z s_k^y s_j^x). \end{aligned} \quad (\text{A6})$$

The derivation above requires a sufficiently small pulse separation τ to ignore higher order terms $\mathcal{O}(\tau^3)$. Since our scheme is focused on the collective part of the model, we can obtain the requirement of τ by writing down the collective part of the original Hamiltonian (1):

$$H_{\text{coll}} = \chi_{\text{coll}} S_z^2, \quad (\text{A7})$$

where the constant terms are neglected and the collective interaction strength reads

$$\chi_{\text{coll}} = \frac{1}{N(N-1)} \sum_{j \neq k} K_{jk} = \frac{K}{N(N-1)} \sum_{j \neq k} \frac{1}{r_{jk}^\alpha}. \quad (\text{A8})$$

Consider large systems, we can estimate the collective interaction strength by replacing the summation in Eq. (A8) with an integral. For 1-dimensional lattice the result is

$$\chi_{\text{coll}}^{d=1} \approx K \frac{2}{L} \int_1^{L/2} dr \frac{1}{r^\alpha} = \begin{cases} \frac{2K}{(1-\alpha)L} \left[\left(\frac{L}{2}\right)^{1-\alpha} - 1 \right] & \alpha \neq 1, \\ \frac{2K}{L} \ln\left(\frac{L}{2}\right) & \alpha = 1. \end{cases} \quad (\text{A9})$$

For 2-dimensional case

$$\chi_{\text{coll}}^{d=2} \approx K \frac{1}{L^2} 2\pi \int_1^{L/2} r dr \frac{1}{r^\alpha} = \begin{cases} \frac{2\pi K}{(2-\alpha)L^2} \left[\left(\frac{L}{2}\right)^{2-\alpha} - 1 \right] & \alpha \neq 2, \\ \frac{2\pi K}{L^2} \ln\left(\frac{L}{2}\right) & \alpha = 2. \end{cases} \quad (\text{A10})$$

It gives the scaling law of the collective interaction strength:

$$\chi_{\text{coll}} \sim \begin{cases} KL^{-\alpha} & \alpha < d, \\ KL^{-d} \ln L & \alpha = d, \\ KL^{-d} & \alpha > d, \end{cases} \quad (\text{A11})$$

where L is the length of the lattice. According to Ref. [61], the requirement for ignoring higher order terms is given by $\chi_{\text{coll}}\tau N/2 \ll 1$. As a result, the critical pulse separation τ_{crit} should satisfy

$$K\tau_{\text{crit}} \sim \begin{cases} L^{-(d-\alpha)} & \alpha < d, \\ (\ln L)^{-1} & \alpha = d, \\ L^0 & \alpha > d. \end{cases} \quad (\text{A12})$$

Appendix B: Zero-momentum/finite-momentum decomposition

In this Appendix, we give the detailed derivation of the zero-momentum/finite-momentum decomposition of the effective Hamiltonian (12), as well as the analytical expression of the spin-wave excitations (16).

1. Zero-momentum component

The zero-momentum component of H_{eff} is its projection in the Dicke manifold $\{|M\rangle\}$:

$$[H_{\text{eff}}]_{\text{ZM}} = \sum_{M, M'} \langle M | H_{\text{eff}} | M' \rangle |M\rangle \langle M'|. \quad (\text{B1})$$

Taking advantage of the permutational symmetry of Dicke states, for $j \neq k$ we have

$$\begin{aligned} [\mathbf{s}_j \cdot \mathbf{s}_k]_{\text{ZM}} &= \sum_{M, M'} \langle M | \mathbf{s}_j \cdot \mathbf{s}_k | M' \rangle |M\rangle \langle M'| \\ &= \frac{1}{N(N-1)} \sum_{M, M'} \langle M | \sum_{j \neq k} \mathbf{s}_j \cdot \mathbf{s}_k | M' \rangle |M\rangle \langle M'|, \end{aligned} \quad (\text{B2})$$

and, for mutually distinct j, k, l ,

$$\begin{aligned} [s_j^x s_k^y s_l^z + s_l^z s_k^y s_j^x]_{\text{ZM}} &= \sum_{M, M'} \langle M | s_j^x s_k^y s_l^z + s_l^z s_k^y s_j^x | M' \rangle |M\rangle \langle M'| \\ &= \frac{1}{N(N-1)(N-2)} \sum_{M, M'} \langle M | \sum_{[j, k, l]} (s_j^x s_k^y s_l^z + s_l^z s_k^y s_j^x) | M' \rangle |M\rangle \langle M'|. \end{aligned} \quad (\text{B3})$$

Noticed that

$$\sum_{j \neq k} \mathbf{s}_j \cdot \mathbf{s}_k = \sum_{j,k} \mathbf{s}_j \cdot \mathbf{s}_k - \sum_j \mathbf{s}_j^2 = \mathbf{S}^2 - \frac{3}{4}N, \quad (\text{B4})$$

$$\begin{aligned} \sum_{[j,k,l]} (s_j^x s_k^y s_l^z + s_l^z s_k^y s_j^x) &= \sum_{j,k,l} (s_j^x s_k^y s_l^z + s_l^z s_k^y s_j^x) - \sum_j (s_j^x s_j^y s_j^z + s_j^z s_j^y s_j^x) \\ &\quad - \sum_{j \neq k} (s_j^x s_k^y s_k^z + s_k^z s_k^y s_j^x) - \sum_{j \neq l} (s_j^x s_j^y s_l^z + s_l^z s_j^y s_j^x) - \sum_{k \neq l} (s_l^x s_k^y s_l^z + s_l^z s_k^y s_l^x) \\ &= S_x S_y S_z + S_z S_y S_x, \end{aligned} \quad (\text{B5})$$

after dropping constants we have

$$H_{\text{ZM}} = [H_{\text{eff}}]_{\text{ZM}} = \frac{1}{3} \lambda K^2 \tau (J_x J_y J_z + J_z J_y J_x), \quad (\text{B6})$$

where $\mathbf{J} = \sum_{M,M'} |M\rangle \langle M| \mathbf{S} |M'\rangle \langle M'|$ is a macroscopic spin operator with a fixed spin length $J = N/2$, and

$$\begin{aligned} \lambda &= \frac{1}{N(N-1)(N-2)} \sum_{[j,k,l]} \left(\frac{1}{r_{jl}^\alpha} \frac{1}{r_{kl}^\alpha} + \frac{1}{r_{jk}^\alpha} \frac{1}{r_{lk}^\alpha} - \frac{1}{r_{kj}^\alpha} \frac{1}{r_{lj}^\alpha} \right) \\ &= \frac{1}{N(N-1)(N-2)} \sum_{[j,k,l]} \frac{1}{r_{jl}^\alpha} \frac{1}{r_{kl}^\alpha}. \end{aligned} \quad (\text{B7})$$

2. Finite-momentum component

The finite-momentum component of H_{eff} is obtained by expressing it in forms of $b_{\mathbf{q}}$, $b_{\mathbf{q}}^\dagger$ and taking the summation of $\mathbf{q} \neq 0$. For convenience, we explicitly split the effective Hamiltonian as

$$H_{\text{eff}} = H_0 + H_1, \quad (\text{B8})$$

including the zeroth-order Heisenberg interaction

$$H_0 = \frac{1}{3} \sum_{j \neq k} K_{jk} \mathbf{s}_j \cdot \mathbf{s}_k, \quad (\text{B9})$$

and the first-order effective three-body interaction

$$H_1 = \frac{1}{3} \tau \sum_{[j,k,l]} K_{[j,k,l]} (s_j^x s_k^y s_l^z + s_l^z s_k^y s_j^x). \quad (\text{B10})$$

To derive the finite-momentum component, we begin by substituting the HP transformation (8) into H_{eff} . Assuming the finite-momentum excitations are weak enough, we keep it up to quadratic terms of the bosonic operators and obtain

$$\begin{aligned} H_0 &\simeq -\frac{1}{12} \sum_{j \neq k} K_{jk} \left[1 - 2 (b_j^\dagger b_j + b_k^\dagger b_k) + (b_j + b_j^\dagger) (b_k + b_k^\dagger) - (b_j - b_j^\dagger) (b_k - b_k^\dagger) \right] \\ &= -\frac{1}{12} \sum_{j \neq k} K_{jk} + \frac{1}{6} \sum_{j \neq k} K_{jk} (b_j^\dagger b_j + b_k^\dagger b_k) - \frac{1}{6} \sum_{j \neq k} K_{jk} (b_j^\dagger b_k + b_k^\dagger b_j), \end{aligned} \quad (\text{B11})$$

and

$$\begin{aligned} H_1 &\simeq -i \frac{\tau}{24} \sum_{[j,k,l]} K_{[j,k,l]} \left[(b_j + b_j^\dagger) (b_k - b_k^\dagger) + (b_k - b_k^\dagger) (b_j + b_j^\dagger) \right] \\ &= -i \frac{\tau}{12} \sum_{[j,k,l]} K_{[j,k,l]} (b_j b_k - b_j^\dagger b_k^\dagger + b_j^\dagger b_k - b_k^\dagger b_j). \end{aligned} \quad (\text{B12})$$

The above expression is then rewritten in momentum space as

$$\begin{aligned}
H_0 &\simeq -\frac{1}{12} \sum_{j \neq k} K_{jk} + \frac{1}{3N} \sum_{j \neq k} K_{jk} \sum_{\mathbf{q}, \mathbf{q}'} e^{-i(\mathbf{q}-\mathbf{q}') \cdot \mathbf{r}_j} b_{\mathbf{q}}^\dagger b_{\mathbf{q}'} - \frac{1}{3N} \sum_{j \neq k} K_{jk} \sum_{\mathbf{q}, \mathbf{q}'} e^{-i(\mathbf{q} \cdot \mathbf{r}_j - \mathbf{q}' \cdot \mathbf{r}_k)} b_{\mathbf{q}}^\dagger b_{\mathbf{q}'}, \\
H_1 &\simeq -i \frac{\tau}{12N} \sum_{[j,k,l]} K_{[j,k,l]} \sum_{\mathbf{q}, \mathbf{q}'} \left[e^{i(\mathbf{q} \cdot \mathbf{r}_j + \mathbf{q}' \cdot \mathbf{r}_k)} b_{\mathbf{q}} b_{\mathbf{q}'} - e^{-i(\mathbf{q} \cdot \mathbf{r}_j + \mathbf{q}' \cdot \mathbf{r}_k)} b_{\mathbf{q}}^\dagger b_{\mathbf{q}'}^\dagger + \left(e^{-i(\mathbf{q} \cdot \mathbf{r}_j - \mathbf{q}' \cdot \mathbf{r}_k)} - e^{i(\mathbf{q} \cdot \mathbf{r}_j - \mathbf{q}' \cdot \mathbf{r}_k)} \right) b_{\mathbf{q}}^\dagger b_{\mathbf{q}'} \right].
\end{aligned} \tag{B13}$$

For periodic lattices we may simplify the expression as

$$\frac{1}{N} \sum_{j \neq k} K_{jk} \sum_{\mathbf{q}, \mathbf{q}'} e^{-i(\mathbf{q}-\mathbf{q}') \cdot \mathbf{r}_j} b_{\mathbf{q}}^\dagger b_{\mathbf{q}'} = \sum_{\mathbf{q}} K_0 b_{\mathbf{q}}^\dagger b_{\mathbf{q}}, \tag{B14}$$

$$\frac{1}{N} \sum_{j \neq k} K_{jk} \sum_{\mathbf{q}, \mathbf{q}'} e^{-i(\mathbf{q} \cdot \mathbf{r}_j - \mathbf{q}' \cdot \mathbf{r}_k)} b_{\mathbf{q}}^\dagger b_{\mathbf{q}'} = \sum_{\mathbf{q}} K_{\mathbf{q}} b_{\mathbf{q}}^\dagger b_{\mathbf{q}}, \tag{B15}$$

where

$$K_{\mathbf{q}} = K \sum_{\substack{\mathbf{r} \\ \mathbf{r} \neq 0}} \frac{1}{r^\alpha} e^{-i\mathbf{q} \cdot \mathbf{r}}. \tag{B16}$$

Also we have

$$\frac{1}{N} \sum_{[j,k,l]} K_{[j,k,l]} \sum_{\mathbf{q}, \mathbf{q}'} e^{i(\mathbf{q} \cdot \mathbf{r}_j + \mathbf{q}' \cdot \mathbf{r}_k)} b_{\mathbf{q}} b_{\mathbf{q}'} = \sum_{\mathbf{q}} (K_{\mathbf{q}}^2 - T_0^2) b_{\mathbf{q}} b_{-\mathbf{q}}, \tag{B17}$$

$$\frac{1}{N} \sum_{[j,k,l]} K_{[j,k,l]} \sum_{\mathbf{q}, \mathbf{q}'} e^{-i(\mathbf{q} \cdot \mathbf{r}_j + \mathbf{q}' \cdot \mathbf{r}_k)} b_{\mathbf{q}}^\dagger b_{\mathbf{q}'}^\dagger = \sum_{\mathbf{q}} (K_{\mathbf{q}}^2 - T_0^2) b_{\mathbf{q}}^\dagger b_{-\mathbf{q}}^\dagger, \tag{B18}$$

$$\frac{1}{N} \sum_{[j,k,l]} K_{[j,k,l]} \sum_{\mathbf{q}, \mathbf{q}'} e^{-i(\mathbf{q} \cdot \mathbf{r}_j - \mathbf{q}' \cdot \mathbf{r}_k)} b_{\mathbf{q}}^\dagger b_{\mathbf{q}'} = \sum_{\mathbf{q}} (K_{\mathbf{q}}^2 - T_0^2) b_{\mathbf{q}}^\dagger b_{\mathbf{q}}, \tag{B19}$$

$$\frac{1}{N} \sum_{[j,k,l]} K_{[j,k,l]} \sum_{\mathbf{q}, \mathbf{q}'} e^{i(\mathbf{q} \cdot \mathbf{r}_j - \mathbf{q}' \cdot \mathbf{r}_k)} b_{\mathbf{q}}^\dagger b_{\mathbf{q}'} = \sum_{\mathbf{q}} (K_{\mathbf{q}}^2 - T_0^2) b_{\mathbf{q}}^\dagger b_{\mathbf{q}}, \tag{B20}$$

where

$$T_0^2 = K^2 \sum_{\substack{\mathbf{r} \\ \mathbf{r} \neq 0}} \frac{1}{r^{2\alpha}}. \tag{B21}$$

Taking the summation over the $\mathbf{q} \neq 0$ sector, we arrive at the expression of the finite-momentum component

$$\begin{aligned}
H_{\text{SW}} &= -\frac{N}{12} K_0 + \frac{1}{3} \sum_{\mathbf{q} \neq 0} (K_0 - K_{\mathbf{q}}) b_{\mathbf{q}}^\dagger b_{\mathbf{q}} \\
&\quad -i \frac{\tau}{12} \sum_{\mathbf{q} \neq 0} (K_{\mathbf{q}}^2 - T_0^2) \left(b_{\mathbf{q}} b_{-\mathbf{q}} - b_{\mathbf{q}}^\dagger b_{-\mathbf{q}}^\dagger \right),
\end{aligned} \tag{B22}$$

3. Bogoliubov diagonalization of the spin-wave Hamiltonian

The spin-wave Hamiltonian (14) can be exactly diagonalized via Bogoliubov transformation. We first write it in the quadratic form

$$H_{\text{SW}} = \frac{1}{2} \sum_{\mathbf{q} \neq 0} \begin{pmatrix} \beta_{\mathbf{q}}^\dagger \\ \beta_{-\mathbf{q}} \end{pmatrix}^T \begin{pmatrix} A_{\mathbf{q}} & \tau B_{\mathbf{q}} \\ \tau B_{\mathbf{q}} & A_{\mathbf{q}} \end{pmatrix} \begin{pmatrix} \beta_{\mathbf{q}} \\ \beta_{-\mathbf{q}}^\dagger \end{pmatrix}, \quad (\text{B23})$$

where we have neglected the constant term and defined

$$\begin{aligned} A_{\mathbf{q}} &= \frac{1}{3} (K_0 - K_{\mathbf{q}}), & B_{\mathbf{q}} &= \frac{1}{6} (K_{\mathbf{q}}^2 - T_0^2), \\ \beta_{\mathbf{q}} &= e^{-i\frac{\pi}{4}} b_{\mathbf{q}}. \end{aligned} \quad (\text{B24})$$

We introduce the Bogoliubov transformation $\beta_{\mathbf{q}} = (u_{\mathbf{q}} a_{\mathbf{q}} - v_{\mathbf{q}} a_{-\mathbf{q}}^\dagger)$ with

$$\begin{aligned} u_{\mathbf{q}} &= \sqrt{\frac{1}{2} \left(\frac{A_{\mathbf{q}}}{\epsilon_{\mathbf{q}}} + 1 \right)}, \\ v_{\mathbf{q}} &= \text{sgn}(B_{\mathbf{q}}) \sqrt{\frac{1}{2} \left(\frac{A_{\mathbf{q}}}{\epsilon_{\mathbf{q}}} - 1 \right)}, \end{aligned} \quad (\text{B25})$$

where the excitation energy $\epsilon_{\mathbf{q}} = \sqrt{A_{\mathbf{q}}^2 - \tau^2 B_{\mathbf{q}}^2}$. The spin-wave Hamiltonian is then written as

$$H_{\text{SW}} = \sum_{\mathbf{q} \neq 0} \epsilon_{\mathbf{q}} \left(a_{\mathbf{q}}^\dagger a_{\mathbf{q}} + \frac{1}{2} \right). \quad (\text{B26})$$

As a result, we can explicitly write down the time-dependence of $a_{\mathbf{q}}$ as

$$a_{\mathbf{q}}(t) = a_{\mathbf{q}}(0) e^{-i\epsilon_{\mathbf{q}} t}. \quad (\text{B27})$$

Since $\epsilon_{\mathbf{q}} = \epsilon_{-\mathbf{q}}$, we have

$$\begin{aligned} \langle b_{\mathbf{q}}^\dagger b_{\mathbf{q}} \rangle_t &= \langle \beta_{\mathbf{q}}^\dagger \beta_{\mathbf{q}} \rangle_t \\ &= u_{\mathbf{q}}^2 \langle a_{\mathbf{q}}^\dagger a_{\mathbf{q}} \rangle_0 + v_{\mathbf{q}}^2 \langle a_{-\mathbf{q}} a_{-\mathbf{q}}^\dagger \rangle_0 \\ &\quad - u_{\mathbf{q}} v_{\mathbf{q}} \left(\langle a_{\mathbf{q}}^\dagger a_{-\mathbf{q}}^\dagger \rangle_0 e^{2i\epsilon_{\mathbf{q}} t} + \langle a_{-\mathbf{q}} a_{\mathbf{q}} \rangle_0 e^{-2i\epsilon_{\mathbf{q}} t} \right). \end{aligned} \quad (\text{B28})$$

Using the inverse transformation $a_{\mathbf{q}} = u_{\mathbf{q}} \beta_{\mathbf{q}} + v_{\mathbf{q}} \beta_{-\mathbf{q}}^\dagger$ we obtain

$$\begin{aligned} \langle a_{\mathbf{q}}^\dagger a_{\mathbf{q}} \rangle_0 &= u_{\mathbf{q}}^2 \langle \beta_{\mathbf{q}}^\dagger \beta_{\mathbf{q}} \rangle_0 + v_{\mathbf{q}}^2 \langle \beta_{-\mathbf{q}} \beta_{-\mathbf{q}}^\dagger \rangle_0 \\ &\quad + u_{\mathbf{q}} v_{\mathbf{q}} \left(\langle \beta_{\mathbf{q}}^\dagger \beta_{-\mathbf{q}}^\dagger \rangle_0 + \langle \beta_{-\mathbf{q}} \beta_{\mathbf{q}} \rangle_0 \right). \end{aligned} \quad (\text{B29})$$

Since the initial coherent spin state $|\uparrow\rangle^{\otimes N}$ is the vacuum state of all $b_{\mathbf{q}}$, the above expression reduces to

$$\langle a_{\mathbf{q}}^\dagger a_{\mathbf{q}} \rangle_0 = v_{\mathbf{q}}^2. \quad (\text{B30})$$

Similarly we have

$$\langle a_{-\mathbf{q}} a_{-\mathbf{q}}^\dagger \rangle_0 = u_{\mathbf{q}}^2, \quad \langle a_{\mathbf{q}}^\dagger a_{-\mathbf{q}}^\dagger \rangle_0 = \langle a_{-\mathbf{q}} a_{\mathbf{q}} \rangle_0 = u_{\mathbf{q}} v_{\mathbf{q}}. \quad (\text{B31})$$

Substituting them into Eq. (B28), we arrive at the explicit expression of finite-momentum spin-wave excitations:

$$\begin{aligned} \langle b_{\mathbf{q}}^\dagger b_{\mathbf{q}} \rangle_t &= 2u_{\mathbf{q}}^2 v_{\mathbf{q}}^2 [1 - \cos(2\epsilon_{\mathbf{q}} t)] \\ &= \frac{\tau^2}{2} \frac{B_{\mathbf{q}}^2}{A_{\mathbf{q}}^2 - \tau^2 B_{\mathbf{q}}^2} [1 - \cos(2\epsilon_{\mathbf{q}} t)]. \end{aligned} \quad (\text{B32})$$

Appendix C: The scaling law of the suitable pulse separation

The requirement for ignoring finite-momentum excitations is $\tau \ll \min_{\mathbf{q}}[A_{\mathbf{q}}/B_{\mathbf{q}}]$, suggesting that the suitable pulse separation τ_s has the same scaling law with $\min_{\mathbf{q}}[A_{\mathbf{q}}/B_{\mathbf{q}}]$. It can be figured out that the mode with the minimum momentum $\mathbf{q}_1 = (2\pi/L, 0, 0, \dots, 0)$ has the largest excitation. In the following, we study the scaling law of $\min_{\mathbf{q}}[A_{\mathbf{q}}/B_{\mathbf{q}}] = A_{\mathbf{q}_1}/B_{\mathbf{q}_1}$ with the help of continuous approximation

$$\begin{aligned} K_0 &= K \sum_{r \neq 0} \frac{1}{r^\alpha} \approx K \varepsilon^{\alpha-d} \int_{\mathbf{x} \in Z_1^d \setminus Z_\varepsilon^d} d^d x \frac{1}{x^\alpha}, \\ K_{\mathbf{q}_1} &= K \sum_{r \neq 0} \frac{1}{r^\alpha} e^{-i\mathbf{q}_1 \cdot \mathbf{r}} \approx K \varepsilon^{\alpha-d} \int_{\mathbf{x} \in Z_1^d \setminus Z_\varepsilon^d} d^d x \frac{1}{x^\alpha} e^{-i\pi x_1}, \\ T_0^2 &= K^2 \sum_{r \neq 0} \frac{1}{r^{2\alpha}} \approx K^2 \varepsilon^{2\alpha-d} \int_{\mathbf{x} \in Z_1^d \setminus Z_\varepsilon^d} d^d x \frac{1}{x^{2\alpha}}, \end{aligned} \quad (\text{C1})$$

where $\varepsilon = 2/L$ and $Z_y = [-y, y]$.

1. 1-dimensional case

For $d = 1$ we have

$$\begin{aligned} K_0 &\approx K \varepsilon^{\alpha-1} 2 \int_\varepsilon^1 dx \frac{1}{x^\alpha} = K \varepsilon^{\alpha-1} \frac{2}{1-\alpha} (1 - \varepsilon^{1-\alpha}), \\ K_{\mathbf{q}_1} &\approx K \varepsilon^{\alpha-1} 2 \int_\varepsilon^1 dx \frac{1}{x^\alpha} \cos(\pi x) \\ &= K \varepsilon^{\alpha-1} \frac{-i}{\pi} \{(-i\pi)^\alpha [\Gamma(1-\alpha, -i\pi) - \Gamma(1-\alpha, -i\pi\varepsilon)] - (i\pi)^\alpha [\Gamma(1-\alpha, i\pi) - \Gamma(1-\alpha, i\pi\varepsilon)]\}, \\ T_0^2 &\approx K^2 \varepsilon^{2\alpha-1} 2 \int_\varepsilon^1 dx \frac{1}{x^{2\alpha}} = K^2 \varepsilon^{2\alpha-1} \frac{2}{1-2\alpha} (1 - \varepsilon^{1-2\alpha}), \end{aligned} \quad (\text{C2})$$

where the incomplete Gamma function is defined as

$$\Gamma(a, z) = \int_z^\infty t^{a-1} e^{-t} dt. \quad (\text{C3})$$

Utilizing the expansion

$$\Gamma(1-\alpha, -i\pi\varepsilon) = \Gamma(1-\alpha) + \frac{(-i\pi\varepsilon)^{1-\alpha}}{\alpha-1} - \frac{(-i\pi\varepsilon)^{2-\alpha}}{\alpha-2} + \frac{(-i\pi\varepsilon)^{3-\alpha}}{2(\alpha-3)} + \mathcal{O}(\varepsilon^{4-\alpha}), \quad (\text{C4})$$

we can obtain the asymptotic behaviour of $A_{\mathbf{q}_1}/B_{\mathbf{q}_1}$ as

$$\begin{aligned} \frac{A_{\mathbf{q}_1}}{B_{\mathbf{q}_1}} &= 2 \frac{K_0 - K_{\mathbf{q}_1}}{K_{\mathbf{q}_1}^2 - T_0^2} \\ &= \frac{2}{K} \varepsilon^{1-\alpha} \frac{\frac{2}{1-\alpha} + E_\alpha(i\pi) + E_\alpha(-i\pi) - 2 \cos\left(\frac{\alpha-1}{2}\pi\right) \pi^{\alpha-1} \Gamma(1-\alpha) + \frac{\pi^2}{\alpha-3} \varepsilon^{3-\alpha} + \mathcal{O}(\varepsilon^{4-\alpha})}{\left[E_\alpha(i\pi) + E_\alpha(-i\pi) - 2 \cos\left(\frac{\alpha-1}{2}\pi\right) \pi^{\alpha-1} \Gamma(1-\alpha) + \frac{2}{1-\alpha} \varepsilon^{1-\alpha} + \frac{\pi^2}{\alpha-3} \varepsilon^{3-\alpha} + \mathcal{O}(\varepsilon^{4-\alpha})\right]^2 - \frac{2}{1-2\alpha} \varepsilon (1 - \varepsilon^{1-2\alpha})}, \end{aligned} \quad (\text{C5})$$

where we use the exponential integral function

$$E_n(z) = \int_1^\infty \frac{e^{-zt}}{t^n} dt. \quad (\text{C6})$$

For $\alpha < 1$, the lowest-order term in Eq. (C5) is

$$\frac{A_{\mathbf{q}_1}}{B_{\mathbf{q}_1}} \sim \frac{2}{K} \frac{\frac{2}{1-\alpha} + E_\alpha(i\pi) + E_\alpha(-i\pi) - 2 \cos\left(\frac{\alpha-1}{2}\pi\right) \pi^{\alpha-1} \Gamma(1-\alpha)}{\left[E_\alpha(i\pi) + E_\alpha(-i\pi) - 2 \cos\left(\frac{\alpha-1}{2}\pi\right) \pi^{\alpha-1} \Gamma(1-\alpha)\right]^2} \varepsilon^{1-\alpha} \sim K^{-1} L^{\alpha-1}, \quad (\text{C7})$$

for $1 < \alpha < 3$ it is

$$\frac{A_{\mathbf{q}_1}}{B_{\mathbf{q}_1}} \sim \frac{2}{K} \frac{\frac{2}{1-\alpha} + E_\alpha(i\pi) + E_\alpha(-i\pi) - 2 \cos\left(\frac{\alpha-1}{2}\pi\right) \pi^{\alpha-1} \Gamma(1-\alpha)}{\frac{4}{(\alpha-1)^2} - \frac{2}{2\alpha-1}} \varepsilon^{\alpha-1} \sim K^{-1} L^{1-\alpha}, \quad (\text{C8})$$

and for $\alpha > 3$

$$\frac{A_{\mathbf{q}_1}}{B_{\mathbf{q}_1}} \sim \frac{2}{K} \frac{\frac{\pi^2}{\alpha-3}}{\frac{4}{(\alpha-1)^2} - \frac{2}{2\alpha-1}} \varepsilon^2 \sim K^{-1} L^{-2}. \quad (\text{C9})$$

We conclude the scaling law in 1-dimensional case as

$$K\tau_s^{d=1} \sim \begin{cases} L^{-(1-\alpha)} & \alpha < 1, \\ L^{-(\alpha-1)} & 1 < \alpha < 3, \\ L^{-2} & \alpha \geq 3. \end{cases} \quad (\text{C10})$$

Note that at the transition point $\alpha = d = 1$, the result is special:

$$\begin{aligned} K_0 &\approx 2K \int_\varepsilon^1 dx \frac{1}{x} = -2K \ln \varepsilon, \\ K_{\mathbf{q}_1} &\approx 2K \int_\varepsilon^1 dx \frac{1}{x} \cos(\pi x) = 2K [\text{Ci}(\pi) - \text{Ci}(\pi\varepsilon)], \\ T_0^2 &\approx 2K^2 \varepsilon \int_\varepsilon^1 dx \frac{1}{x^2} = 2K^2(1 - \varepsilon), \end{aligned} \quad (\text{C11})$$

where the cosine integral function is defined as

$$\text{Ci}(z) = - \int_z^\infty \frac{\cos(t)}{t} dt, \quad (\text{C12})$$

which has the expansion

$$\text{Ci}(\pi\varepsilon) = \ln(\pi\varepsilon) + \gamma_{\text{Euler}} + \mathcal{O}(\varepsilon^2), \quad (\text{C13})$$

where $\gamma_{\text{Euler}} \approx 0.577$ is the Euler constant. The lowest-order term is now given by

$$\frac{A_{\mathbf{q}_1}}{B_{\mathbf{q}_1}} \sim \frac{1}{K} \frac{\ln \pi + \gamma_{\text{Euler}} - \text{Ci}(\pi)}{(\ln L)^2} \sim K^{-1} (\ln L)^{-2}. \quad (\text{C14})$$

2. 2-dimensional case

In the case of $d = 2$ we have

$$\begin{aligned} K_0 &\approx K \varepsilon^{\alpha-2} 2\pi \int_\varepsilon^1 r dr \frac{1}{r^\alpha} = K \frac{2\pi}{2-\alpha} \varepsilon^{\alpha-2} (1 - \varepsilon^{2-\alpha}), \\ K_{\mathbf{q}_1} &\approx K \varepsilon^{\alpha-2} \int_\varepsilon^1 r dr \frac{1}{r^\alpha} \int_0^{2\pi} d\theta e^{-i\pi r \cos \theta} = K \varepsilon^{\alpha-2} 2\pi \int_\varepsilon^1 r dr \frac{1}{r^\alpha} J_0(\pi r) \\ &= K \frac{2\pi}{2-\alpha} \varepsilon^{\alpha-2} \left[{}_1F_2 \left(1 - \frac{\alpha}{2}; 1, 2 - \frac{\alpha}{2}; -\frac{\pi^2}{4} \right) - \varepsilon^{2-\alpha} {}_1F_2 \left(1 - \frac{\alpha}{2}; 1, 2 - \frac{\alpha}{2}; -\frac{\pi^2}{4} \varepsilon^2 \right) \right], \\ T_0^2 &\approx K^2 \varepsilon^{2\alpha-2} 2\pi \int_\varepsilon^1 r dr \frac{1}{r^{2\alpha}} = K^2 \frac{\pi}{1-\alpha} \varepsilon^{2\alpha-2} (1 - \varepsilon^{2-2\alpha}), \end{aligned} \quad (\text{C15})$$

where we have approximately replaced the region $\mathbf{x} \in Z_1^2 \setminus Z_\varepsilon^2$ with $\varepsilon < |\mathbf{x}| < 1$ to simplify the integral, $J_n(z)$ is the n th-order Bessel function of the first kind, and ${}_pF_q(\{a\}; \{b\}; z)$ is the generalized hypergeometric function

$${}_pF_q(\{a\}; \{b\}; z) = \sum_{k=0}^{\infty} \frac{(a_1)_k (a_2)_k \dots (a_p)_k}{(b_1)_k (b_2)_k \dots (b_q)_k} \frac{z^k}{k!}, \quad (\text{C16})$$

which is defined with the Pochhammer symbol

$$(a)_n = \begin{cases} 1 & n = 0, \\ a(a+1)(a+2)\dots(a+n-1) & n > 0. \end{cases} \quad (\text{C17})$$

We can expand the expression using

$${}_1F_2\left(1 - \frac{\alpha}{2}; 1, 2 - \frac{\alpha}{2}; -\frac{1}{4}\pi^2\varepsilon^2\right) = 1 - \frac{\alpha - 2}{\alpha - 4} \frac{\pi^2}{4} \varepsilon^2 + \mathcal{O}(\varepsilon^4), \quad (\text{C18})$$

so that

$$\begin{aligned} \frac{A_{\mathbf{q}_1}}{B_{\mathbf{q}_1}} &= 2 \frac{K_0 - K_{\mathbf{q}_1}}{K_{\mathbf{q}_1}^2 - T_0^2} \\ &= \frac{2}{\pi K} \varepsilon^{2-\alpha} \frac{\frac{2}{2-\alpha} \left[1 - {}_1F_2\left(1 - \frac{\alpha}{2}; 1, 2 - \frac{\alpha}{2}; -\frac{\pi^2}{4}\right) \right] + \frac{2}{\alpha-4} \frac{\pi^2}{4} \varepsilon^{4-\alpha} + \mathcal{O}(\varepsilon^{6-\alpha})}{\left(\frac{4}{(2-\alpha)^2} \left[{}_1F_2\left(1 - \frac{\alpha}{2}; 1, 2 - \frac{\alpha}{2}; -\frac{\pi^2}{4}\right) - \varepsilon^{2-\alpha} + \frac{\alpha-2}{\alpha-4} \frac{\pi^2}{4} \varepsilon^{4-\alpha} + \mathcal{O}(\varepsilon^{6-\alpha}) \right]^2 - \frac{1}{(1-\alpha)\pi} \varepsilon^2 (1 - \varepsilon^{2-2\alpha}) \right)}. \end{aligned} \quad (\text{C19})$$

For $\alpha < 2$, the lowest order term is given by

$$\begin{aligned} \frac{A_{\mathbf{q}_1}}{B_{\mathbf{q}_1}} &\sim \frac{2 - \alpha}{2\pi K} \frac{1 - {}_1F_2\left(1 - \frac{\alpha}{2}; 1, 2 - \frac{\alpha}{2}; -\frac{\pi^2}{4}\right)}{\left[{}_1F_2\left(1 - \frac{\alpha}{2}; 1, 2 - \frac{\alpha}{2}; -\frac{\pi^2}{4}\right) \right]^2} \varepsilon^{2-\alpha} \\ &\sim K^{-1} L^{\alpha-2}, \end{aligned} \quad (\text{C20})$$

for $2 < \alpha < 4$ it is

$$\begin{aligned} \frac{A_{\mathbf{q}_1}}{B_{\mathbf{q}_1}} &\sim \frac{2}{(2-\alpha)\pi K} \frac{1 - {}_1F_2\left(1 - \frac{\alpha}{2}; 1, 2 - \frac{\alpha}{2}; -\frac{\pi^2}{4}\right)}{\left(\frac{4}{(\alpha-2)^2} - \frac{1}{(\alpha-1)\pi}\right)} \varepsilon^{\alpha-2} \\ &\sim K^{-1} L^{2-\alpha}, \end{aligned} \quad (\text{C21})$$

and for $\alpha > 4$

$$\frac{A_{\mathbf{q}_1}}{B_{\mathbf{q}_1}} \sim \frac{2}{(\alpha-4)\pi K} \frac{\frac{\pi^2}{4}}{\left(\frac{4}{(\alpha-2)^2} - \frac{1}{(\alpha-1)\pi}\right)} \varepsilon^2 \sim K^{-1} L^{-2}. \quad (\text{C22})$$

The scaling law for 2-dimensional case is

$$K\tau_s^{d=2} \sim \begin{cases} L^{-(2-\alpha)} & \alpha < 2, \\ L^{-(\alpha-2)} & 2 < \alpha < 4, \\ L^{-2} & \alpha \geq 4. \end{cases} \quad (\text{C23})$$

At the transition point $\alpha = d = 2$, the result becomes

$$\begin{aligned} K_0 &\approx 2\pi K \int_{\varepsilon}^1 dx \frac{1}{r} = -2\pi K \ln \varepsilon, \\ K_{\mathbf{q}_1} &\approx 2\pi K \int_{\varepsilon}^1 dr \frac{1}{r} J_0(\pi r) = -\pi K \left[G_{1,3}^{2,0} \left(\frac{\pi^2}{4} \middle| 1, 0, 0 \right) - G_{1,3}^{2,0} \left(\frac{\pi^2 \varepsilon^2}{4} \middle| 1, 0, 0 \right) \right], \\ T_0^2 &\approx 2\pi K^2 \varepsilon^2 \int_{\varepsilon}^1 dr \frac{1}{r^3} = \pi K^2 (1 - \varepsilon^2), \end{aligned} \quad (\text{C24})$$

where $G_{p,q}^{m,n} \left(z \middle| \begin{smallmatrix} a_1, \dots, a_p \\ b_1, \dots, b_q \end{smallmatrix} \right)$ is the Meijer G-function

$$G_{p,q}^{m,n} \left(z \middle| \begin{smallmatrix} a_1, \dots, a_p \\ b_1, \dots, b_q \end{smallmatrix} \right) = \frac{1}{2\pi i} \int \frac{\Gamma(1 - a_1 - s) \dots \Gamma(1 - a_n - s) \Gamma(b_1 + s) \dots \Gamma(b_m + s)}{\Gamma(a_{n+1} + s) \dots \Gamma(a_p + s) \Gamma(1 - b_{m+1} - s) \dots \Gamma(1 - b_p - s)} z^{-s} ds, \quad (\text{C25})$$

which can be expanded as

$$G_{1,3}^{2,0} \left(\frac{\pi^2 \varepsilon^2}{4} \middle|_{0,0,0}^1 \right) = -2 \ln \left(\frac{\pi}{2} \varepsilon \right) - 2\gamma_{\text{Euler}} + \mathcal{O}(\varepsilon^2). \quad (\text{C26})$$

Thus we obtain

$$\frac{A_{\mathbf{q}_1}}{B_{\mathbf{q}_1}} \sim \frac{1}{\pi K} \frac{\ln \frac{\pi}{2} + \gamma_{\text{Euler}} + \frac{1}{2} G_{1,3}^{2,0} \left(\frac{\pi^2}{4} \middle|_{0,0,0}^1 \right)}{(\ln L)^2} \sim K^{-1} (\ln L)^{-2}. \quad (\text{C27})$$

3. The uniform expression

It is easy to find the scaling law of τ_s —for both $d = 1$ and $d = 2$ —can be expressed in a uniform way

$$K\tau_s \sim \begin{cases} L^{-(d-\alpha)} & \alpha < d, \\ L^{-(\alpha-d)} & d < \alpha < d+2, \\ L^{-2} & \alpha \geq d+2. \end{cases} \quad (\text{C28})$$

At the transition point $\alpha = d$, the power-law form collapses and changes into the logarithmic form:

$$K\tau_s^{\alpha=d} \sim (\ln L)^{-2}. \quad (\text{C29})$$

Appendix D: The scaling law of the total evolution time

For the zero-momentum collective-spin XYZ Hamiltonian (13), the evolution time to create the GHZ-like state is given by [61]

$$Kt_c \simeq \frac{6 \ln N}{\lambda K \tau N^2}. \quad (\text{D1})$$

Since the scaling law of the pulse separation has been obtained as $K\tau \sim L^{-\mu}$, the remaining step to estimate the scaling behavior of the evolution time t_c is to determine the parameter λ , which characterizes the average three-body interaction strength. Using the similar method to the one in Appendix C, we can approximately convert Eq. (B7) into an integral

$$\begin{aligned} \lambda^{d=1} &\approx \frac{1}{N^2} \left(2 \int_1^{L/2} dr \frac{1}{r^\alpha} \right)^2, \\ \lambda^{d=2} &\approx \frac{1}{N^2} \left(\int_1^{L/2} 2\pi r dr \frac{1}{r^\alpha} \right)^2. \end{aligned} \quad (\text{D2})$$

The scaling law of λ can be directly obtained from the above equation, which gives

$$\lambda \sim \begin{cases} L^{-2\alpha} & \alpha < d, \\ L^{-2d} (\ln L)^2 & \alpha = d, \\ L^{-2d} & \alpha > d. \end{cases} \quad (\text{D3})$$

Substituting this result into Eq. (D1), along with the result (22), we immediately find the scaling law of the

evolution time: $t_c \sim L^{-\nu} \ln L$ with

$$\nu = \begin{cases} d - \alpha & \alpha < d + 2, \\ -2 & \alpha \geq d + 2. \end{cases} \quad (\text{D4})$$

Appendix E: The power-law exponent of the suitable pulse separation

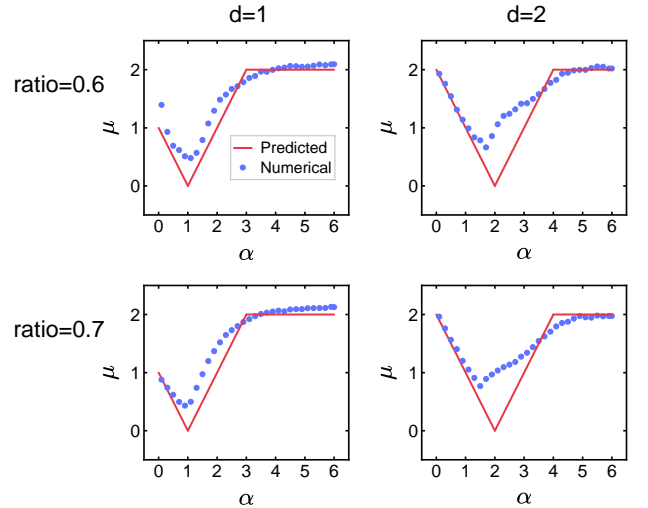


FIG. 6. The power-law exponent μ of the suitable pulse separation τ_s , approximately obeying $\tau_s \sim L^{-\mu}$ with μ relying on α . Numerical results are fitted using different critical ratios $F_Q/F_Q^{\text{eff}} = 0.6, 0.7$.

In Fig. 4, we have verified the predicted power-law exponent μ by fixing $F_Q/F_Q^{\text{eff}} = 0.8$ and numerically fitting it. Fitted results using other ratios $F_Q/F_Q^{\text{eff}} = 0.6, 0.7$

are provided in Fig. 6. It is obvious that different ratios give very similar results, showing that the scaling behavior does not rely on the artificial choice of the critical ratio.

-
- [1] F. Arute, K. Arya, R. Babbush, *et al.*, Quantum supremacy using a programmable superconducting processor, *Nature* **574**, 505 (2019).
- [2] S. J. Evered, D. Bluvstein, M. Kalinowski, S. Ebadi, T. Manovitz, H. Zhou, S. H. Li, A. A. Geim, T. T. Wang, N. Maskara, H. Levine, G. Semeghini, M. Greiner, V. Vuletic, and M. D. Lukin, High-fidelity parallel entangling gates on a neutral-atom quantum computer, *Nature* **622**, 268 (2023).
- [3] S. A. Moses, C. H. Baldwin, M. S. Allman, *et al.*, A race-track trapped-ion quantum processor, *Phys. Rev. X* **13**, 041052 (2023).
- [4] P. Scholl, M. Schuler, H. J. Williams, A. A. Eberharter, D. Barredo, K.-N. Schymik, V. Lienhard, L.-P. Henry, T. C. Lang, T. Lahaye, A. M. Laeuchli, and A. Browaeys, Quantum simulation of 2d antiferromagnets with hundreds of rydberg atoms, *Nature* **595**, 233 (2021).
- [5] S. L. Cornish, M. R. Tarbutt, and K. R. A. Hazzard, Quantum computation and quantum simulation with ultracold molecules, *Nat. Phys.* **20**, 730 (2024).
- [6] S. A. Guo, Y. K. Wu, J. Ye, L. Zhang, W. Q. Lian, R. Yao, Y. Wang, R. Y. Yan, Y. J. Yi, Y. L. Xu, B. W. Li, Y. H. Hou, Y. Z. Xu, W. X. Guo, C. Zhang, B. X. Qi, Z. C. Zhou, L. He, and L. M. Duan, A site-resolved two-dimensional quantum simulator with hundreds of trapped ions, *Nature* **630**, 613 (2024).
- [7] M. A. Norcia, A. W. Young, W. J. Eckner, E. Oelker, J. Ye, and A. M. Kaufman, Seconds-scale coherence on an optical clock transition in a tweezer array, *Science* **366**, 93 (2019).
- [8] I. S. Madjarov, A. Cooper, A. L. Shaw, J. P. Covey, V. Schkolnik, T. H. Yoon, J. R. Williams, and M. Endres, An atomic-array optical clock with single-atom readout, *Phys. Rev. X* **9**, 041052 (2019).
- [9] W. J. Eckner, N. D. Oppong, A. Cao, A. W. Young, W. R. Milner, J. M. Robinson, J. Ye, and A. M. Kaufman, Realizing spin squeezing with rydberg interactions in an optical clock, *Nature* **621**, 734 (2023).
- [10] V. Giovannetti, S. Lloyd, and L. Maccone, Quantum-enhanced measurements: Beating the standard quantum limit, *Science* **306**, 1330 (2004).
- [11] S. Cao, B. Wu, F. Chen, M. Gong, Y. Wu, Y. Ye, C. Zha, H. Qian, C. Ying, S. Guo, Q. Zhu, H.-L. Huang, Y. Zhao, S. Li, S. Wang, J. Yu, D. Fan, D. Wu, H. Su, H. Deng, H. Rong, Y. Li, K. Zhang, T.-H. Chung, F. Liang, J. Lin, Y. Xu, L. Sun, C. Guo, N. Li, Y.-H. Huo, C.-Z. Peng, C.-Y. Lu, X. Yuan, X. Zhu, and J.-W. Pan, Generation of genuine entanglement up to 51 superconducting qubits, *Nature* **619**, 738 (2023).
- [12] M. Kitagawa and M. Ueda, Squeezed spin states, *Phys. Rev. A* **47**, 5138 (1993).
- [13] D. J. Wineland, J. J. Bollinger, W. M. Itano, and D. J. Heinzen, Squeezed atomic states and projection noise in spectroscopy, *Phys. Rev. A* **50**, 67 (1994).
- [14] J. Esteve, C. Gross, A. Weller, S. Giovanazzi, and M. K. Oberthaler, Squeezing and entanglement in a bose-einstein condensate, *Nature* **455**, 1216 (2008).
- [15] G.-R. Jin, Y.-C. Liu, and W.-M. Liu, Spin squeezing in a generalized one-axis twisting model, *New J. Phys.* **11**, 073049 (2009).
- [16] J. Ma, X. Wang, C. Sun, and F. Nori, Quantum spin squeezing, *Phys. Rep.* **509**, 89 (2011).
- [17] Y. C. Liu, Z. F. Xu, G. R. Jin, and L. You, Spin squeezing: Transforming one-axis twisting into two-axis twisting, *Phys. Rev. Lett.* **107**, 013601 (2011).
- [18] F. Chen, J.-J. Chen, L.-N. Wu, Y.-C. Liu, and L. You, Extreme spin squeezing from deep reinforcement learning, *Phys. Rev. A* **100**, 041801(R) (2019).
- [19] H. Bao, J. Duan, S. Jin, X. Lu, P. Li, W. Qu, M. Wang, I. Novikova, E. E. Mikhailov, K.-F. Zhao, K. Molmer, H. Shen, and Y. Xiao, Spin squeezing of 10^{11} atoms by prediction and retrodiction measurements, *Nature* **581**, 159 (2020).
- [20] L.-G. Huang, F. Chen, X. Li, Y. Li, R. Lu, and Y.-C. Liu, Dynamic synthesis of heisenberg-limited spin squeezing, *npj Quant. Inform.* **7**, 168 (2021).
- [21] L.-G. Huang, X. Zhang, Y. Wang, Z. Hua, Y. Tang, and Y.-C. Liu, Heisenberg-limited spin squeezing in coupled spin systems, *Phys. Rev. A* **107**, 042613 (2023).
- [22] Z. Hu, Q. Li, X. Zhang, L.-G. Huang, H.-b. Zhang, and Y.-C. Liu, Spin squeezing with arbitrary quadratic collective-spin interactions, *Phys. Rev. A* **108**, 023722 (2023).
- [23] C. Gross, T. Zibold, E. Nicklas, J. Esteve, and M. K. Oberthaler, Nonlinear atom interferometer surpasses classical precision limit, *Nature* **464**, 1165 (2010).
- [24] M. F. Riedel, P. Boehi, Y. Li, T. W. Haensch, A. Sinatra, and P. Treutlein, Atom-chip-based generation of entanglement for quantum metrology, *Nature* **464**, 1170 (2010).
- [25] L. Pezzè, A. Smerzi, M. K. Oberthaler, R. Schmied, and P. Treutlein, Quantum metrology with nonclassical states of atomic ensembles, *Rev. Mod. Phys.* **90**, 035005 (2018).
- [26] G. P. Greve, C. Luo, B. Wu, and J. K. Thompson, Entanglement-enhanced matter-wave interferometry in a high-finesse cavity, *Nature* **610**, 472 (2022).
- [27] T.-W. Mao, Q. Liu, X.-W. Li, J.-H. Cao, F. Chen, W.-X. Xu, M. K. Tey, Y.-X. Huang, and L. You, Quantum-enhanced sensing by echoing spin-nematic squeezing in atomic bose-einstein condensate, *Nat. Phys.* **19**, 1585 (2023).
- [28] J. M. Robinson, M. Miklos, Y. M. Tso, C. J. Kennedy, T. Bothwell, D. Kedar, J. K. Thompson, and J. Ye, Direct comparison of two spin-squeezed optical clock ensembles at the 10^{-17} level, *Nat. Phys.* **20**, 208 (2024).
- [29] M. Foss-Feig, Z.-X. Gong, A. V. Gorshkov, and C. W. Clark, *Entanglement and spin-squeezing without infinite-range interactions* (2016), arXiv:1612.07805 [cond-mat.quant-gas].
- [30] J. G. Bohnet, B. C. Sawyer, J. W. Britton, M. L. Wall,

- A. M. Rey, M. Foss-Feig, and J. J. Bollinger, Quantum spin dynamics and entanglement generation with hundreds of trapped ions, *Science* **352**, 1297 (2016).
- [31] M. A. Perlin, C. Qu, and A. M. Rey, Spin squeezing with short-range spin-exchange interactions, *Phys. Rev. Lett.* **125**, 223401 (2020).
- [32] T. Comparin, F. Mezzacapo, and T. Roscilde, Robust spin squeezing from the tower of states of $u(1)$ -symmetric spin hamiltonians, *Phys. Rev. A* **105**, 022625 (2022).
- [33] J. T. Young, S. R. Muleady, M. A. Perlin, A. M. Kaufman, and A. M. Rey, Enhancing spin squeezing using soft-core interactions, *Phys. Rev. Res.* **5**, L012033 (2023).
- [34] G. Bornet, G. Emperauger, C. Chen, B. Ye, M. Block, M. Bintz, J. A. Boyd, D. Barredo, T. Comparin, F. Mezzacapo, T. Roscilde, T. Lahaye, N. Y. Yao, and A. Browaeys, Scalable spin squeezing in a dipolar rydberg atom array, *Nature* **621**, 728 (2023).
- [35] J. Franke, S. R. Muleady, R. Kaubruegger, F. Kranzl, R. Blatt, A. M. Rey, M. K. Joshi, and C. F. Roos, Quantum-enhanced sensing on optical transitions through finite-range interactions, *Nature* **621**, 740 (2023).
- [36] M. Block, B. Ye, B. Roberts, S. Chern, W. Wu, Z. Wang, L. Pollet, E. J. Davis, B. I. Halperin, and N. Y. Yao, Scalable spin squeezing from finite-temperature easy-plane magnetism, *Nat. Phys.* **20**, 1575 (2024).
- [37] D. Greenberger, M. Horne, A. Shimony, and A. Zeilinger, Bell's theorem without inequalities, *Am. J. Phys.* **58**, 1131 (1990).
- [38] J. J. Bollinger, W. M. Itano, D. J. Wineland, and D. J. Heinzen, Optimal frequency measurements with maximally correlated states, *Phys. Rev. A* **54**, R4649 (1996).
- [39] D. Leibfried, M. Barrett, T. Schaetz, J. Britton, J. Chiaverini, W. Itano, J. Jost, C. Langer, and D. Wineland, Toward heisenberg-limited spectroscopy with multiparticle entangled states, *Science* **304**, 1476 (2004).
- [40] F. Fröwis, P. Sekatski, W. Dür, N. Gisin, and N. Sangouard, Macroscopic quantum states: Measures, fragility, and implementations, *Rev. Mod. Phys.* **90**, 025004 (2018).
- [41] N. D. Mermin, Extreme quantum entanglement in a superposition of macroscopically distinct states, *Phys. Rev. Lett.* **65**, 1838 (1990).
- [42] C. Song, K. Xu, W. Liu, C.-p. Yang, S.-B. Zheng, H. Deng, Q. Xie, K. Huang, Q. Guo, L. Zhang, P. Zhang, D. Xu, D. Zheng, X. Zhu, H. Wang, Y.-A. Chen, C.-Y. Lu, S. Han, and J.-W. Pan, 10-qubit entanglement and parallel logic operations with a superconducting circuit, *Phys. Rev. Lett.* **119**, 180511 (2017).
- [43] C. Song, K. Xu, H. Li, Y.-R. Zhang, X. Zhang, W. Liu, Q. Guo, Z. Wang, W. Ren, J. Hao, H. Feng, H. Fan, D. Zheng, D.-W. Wang, H. Wang, and S.-Y. Zhu, Generation of multicomponent atomic schrödinger cat states of up to 20 qubits, *Science* **365**, 574 (2019).
- [44] Z. Bao, S. Xu, Z. Song, K. Wang, L. Xiang, Z. Zhu, J. Chen, F. Jin, X. Zhu, Y. Gao, Y. Wu, C. Zhang, N. Wang, Y. Zou, Z. Tan, A. Zhang, Z. Cui, F. Shen, J. Zhong, T. Li, J. Deng, X. Zhang, H. Dong, P. Zhang, Y.-R. Liu, L. Zhao, J. Hao, H. Li, Z. Wang, C. Song, Q. Guo, B. Huang, and H. Wang, Creating and controlling global greenberger-horne-zeilinger entanglement on quantum processors, *Nat. Commun.* **15**, 8823 (2024).
- [45] T. Monz, P. Schindler, J. T. Barreiro, M. Chwalla, D. Nigg, W. A. Coish, M. Harlander, W. Hänsel, M. Henrich, and R. Blatt, 14-qubit entanglement: Creation and coherence, *Phys. Rev. Lett.* **106**, 130506 (2011).
- [46] T. Choi, S. Debnath, T. A. Manning, C. Figgatt, Z.-X. Gong, L.-M. Duan, and C. Monroe, Optimal quantum control of multimode couplings between trapped ion qubits for scalable entanglement, *Phys. Rev. Lett.* **112**, 190502 (2014).
- [47] A. Omran, H. Levine, A. Keesling, G. Semeghini, T. T. Wang, S. Ebadi, H. Bernien, A. S. Zibrov, H. Pichler, S. Choi, J. Cui, M. Rossignolo, P. Rembold, S. Montangero, T. Calarco, M. Endres, M. Greiner, V. Vuletić, and M. D. Lukin, Generation and manipulation of schrödinger cat states in rydberg atom arrays, *Science* **365**, 570 (2019).
- [48] X.-L. Wang, L.-K. Chen, W. Li, H.-L. Huang, C. Liu, C. Chen, Y.-H. Luo, Z.-E. Su, D. Wu, Z.-D. Li, H. Lu, Y. Hu, X. Jiang, C.-Z. Peng, L. Li, N.-L. Liu, Y.-A. Chen, C.-Y. Lu, and J.-W. Pan, Experimental ten-photon entanglement, *Phys. Rev. Lett.* **117**, 210502 (2016).
- [49] X.-L. Wang, Y.-H. Luo, H.-L. Huang, M.-C. Chen, Z.-E. Su, C. Liu, C. Chen, W. Li, Y.-Q. Fang, X. Jiang, J. Zhang, L. Li, N.-L. Liu, C.-Y. Lu, and J.-W. Pan, 18-qubit entanglement with six photons' three degrees of freedom, *Phys. Rev. Lett.* **120**, 260502 (2018).
- [50] H. Kaufmann, T. Ruster, C. T. Schmiegelow, M. A. Luda, V. Kaushal, J. Schulz, D. von Lindenfels, F. Schmidt-Kaler, and U. G. Poschinger, Scalable creation of long-lived multipartite entanglement, *Phys. Rev. Lett.* **119**, 150503 (2017).
- [51] K. X. Wei, I. Lauer, S. Srinivasan, N. Sundaresan, D. T. McClure, D. Toyli, D. C. McKay, J. M. Gambetta, and S. Sheldon, Verifying multipartite entangled greenberger-horne-zeilinger states via multiple quantum coherences, *Phys. Rev. A* **101**, 032343 (2020).
- [52] G. J. Mooney, G. A. L. White, C. D. Hill, and L. C. L. Hollenberg, Generation and verification of 27-qubit greenberger-horne-zeilinger states in a superconducting quantum computer, *J. Phys. Commun.* **5**, 095004 (2021).
- [53] Y. Lu, S. Zhang, K. Zhang, W. Chen, Y. Shen, J. Zhang, J.-N. Zhang, and K. Kim, Global entangling gates on arbitrary ion qubits, *Nature* **572**, 363 (2019).
- [54] A. Cao, W. J. Eckner, T. L. Yelin, A. W. Young, S. Jandura, L. Yan, K. Kim, G. Pupillo, J. Ye, N. D. Oppong, and A. M. Kaufman, Multi-qubit gates and schrödinger cat states in an optical clock, *Nature* **634**, 315 (2024).
- [55] J. W. Britton, B. C. Sawyer, A. C. Keith, C. C. J. Wang, J. K. Freericks, H. Uys, M. J. Biercuk, and J. J. Bollinger, Engineered two-dimensional ising interactions in a trapped-ion quantum simulator with hundreds of spins, *Nature* **484**, 489 (2012).
- [56] C. Monroe, W. C. Campbell, L.-M. Duan, Z.-X. Gong, A. V. Gorshkov, P. W. Hess, R. Islam, K. Kim, N. M. Linke, G. Pagano, P. Richerme, C. Senko, and N. Y. Yao, Programmable quantum simulations of spin systems with trapped ions, *Rev. Mod. Phys.* **93**, 025001 (2021).
- [57] P. Schauss, M. Cheneau, M. Endres, T. Fukuhara, S. Hild, A. Omran, T. Pohl, C. Gross, S. Kuhr, and I. Bloch, Observation of spatially ordered structures in a two-dimensional rydberg gas, *Nature* **491**, 87 (2012).
- [58] A. Browaeys and T. Lahaye, Many-body physics with individually controlled rydberg atoms, *Nat. Phys.* **16**, 132 (2020).
- [59] C. Miller, A. N. Carroll, J. Lin, H. Hirzler, H. Gao,

- H. Zhou, M. D. Lukin, and J. Ye, Two-axis twisting using floquet-engineered xyz spin models with polar molecules, *Nature* **633**, 332 (2024).
- [60] P. Frey and S. Rachel, Realization of a discrete time crystal on 57 qubits of a quantum computer, *Sci. Adv.* **8**, eabm7652 (2022).
- [61] X. Zhang, Z. Hu, and Y.-C. Liu, Fast generation of ghz-like states using collective-spin XYZ model, *Phys. Rev. Lett.* **132**, 113402 (2024).
- [62] T. Roscilde, T. Comparin, and F. Mezzacapo, Rotor/spin-wave theory for quantum spin models with $u(1)$ symmetry, *Phys. Rev. B* **108**, 155130 (2023).
- [63] J. Schachenmayer, A. Pikovski, and A. M. Rey, Many-body quantum spin dynamics with monte carlo trajectories on a discrete phase space, *Phys. Rev. X* **5**, 011022 (2015).
- [64] J. T. Reilly, J. D. Wilson, S. B. Jäger, C. Wilson, and M. J. Holland, Optimal generators for quantum sensing, *Phys. Rev. Lett.* **131**, 150802 (2023).
- [65] Y. Chen and X. Zhang, LatticeGHZlike, <https://github.com/simonchenyf/LatticeGHZlike> (2026).